Applied Surface Science Advances 10 (2022) 100264

Contents lists available at ScienceDirect

Applied Surface Science Advances

journal homepage: www.sciencedirect.com/journal/applied-surface-science-advances

Langmuir-Blodgett monolayer of electrochemically synthesized PANI-TiO_2 nanocomposites for MSG biosensor

Devdutt Sharma [a], Hemant Sankar Dutta [b], Marshal Dhayal [a,*]

[a] Nano-Cellular Medicine and Biophysics Laboratory, School of Biomedical Engineering, Indian Institute of Technology (Banaras Hindu University), Varanasi, UP 221005, India
[b] Analytical Chemistry Group, Material Sciences & Technology Division, CSIR-North East Institute of Science & Technology, Jorhat, Assam 785006, India

ARTICLE INFO

Keywords:
Langmuir-Blodgett
Mono-sodium glutamate
Polyaniline-TiO_2 nanocomposite
Cyclic voltammetry
Differential pulse voltammetry
Electrochemical immunosensor

ABSTRACT

Nanocomposites of polyaniline titanium oxide (PANI-TiO_2) have been synthesized by employing the electrochemical technique and their monolayers were prepared on a pre-chemical treated indium tin oxide (ITO) surface through Langmuir-Blodgett (LB) process. The TEM images show the well dispersion of an average ~ 5 nm diameter TiO_2 particles in the film of PANI-TiO_2 with ~ 0.35 nm interatomic spacing of titanium atoms in the anatase crystalline plane (101). X-ray photoelectron (XPS) spectra of LB film of PANI-TiO_2 also confirmed the presence of Ti atoms as a similar observation was also confirmed in energy dispersive X-ray analysis (EDX) analysis of the film surface. Electrochemical conductivity of the PANI-TiO_2 LB films showed enhancement in peak current, and subsequent immobilization of monoclonal antibodies specific to L-glutamic acid was achieved. Differential pulse voltammetry (DPV) measurements showed a linear response in the peak current with MSG concentration varying from 1 nM to 500 μM and 1 μM to 250 μM in the electrolyte and tomato sauce, respectively. The detection sensitivity of the immunosensor was ~ 37 mA/nM.

1. Introduction

In recent years, extensive work has been done on developing high-sensitivity electrochemical biosensors by increasing surface-to-volume ratio and conductivity. Thus, the electrochemical biosensor has gained significant interest in addressing the need to develop rapid, low cost and point-of-care diagnostic systems [1–3]. There have been three areas of interest while addressing the challenges in electrochemical biosensors (i) identifying a suitable choice of materials that serves the objective of achieving higher biocompatible nature with conducting characteristics, (ii) finding appropriate methods for binding these on substrates, and (iii) controlling thickness at the surfaces. In the past, a range of vacuum and non-vacuum-based methods such as chemical vapor deposition [4], physical vapor deposition [5], electrodeposition [6], sol-gel, and many other ways have been used for the deposition of thin films and coatings [7–9]. These provide unique characteristics and control over physico-chemical properties, but the thickness may differ for different deposition methods. The surface modification has also been used to achieve functionalization or deposition of molecular layers through self-assembly had also provided desired binding sites at the surfaces [10–12]. Self-assembly is a spontaneous process that allows the assembly of molecules with a specific binding affinity toward substrates, making better control over the surface thickness possible [13].

Langmuir-Blodgett process has been very commonly used for depositing thin films of organic monomers with better control of thickness [14,15]. The usefulness of Langmuir–Blodgett films has been demonstrated in interfacial nano-architectonics with biomolecules [16], materials, living objects [17], optical gas sensing [18], polymer light-emitting diodes [19], single-molecule nanomagnets [20], and biosensors [21,22]. The deposition of Langmuir–Blodgett film involves the creation of a well-ordered structure of a compact Langmuir monomolecular layer at the air-water interface and subsequently transferring the highly oriented thin film layer onto substrates by the vertical dipping method [23]. This enables the preparation of 2D materials coatings of a single molecular layer with the possibility of incorporating a range of molecules and nanoparticles [24,25]. However, there is limited scope for containing nanoparticles due to their relative higher mass density with molecules participating in this process.

The present study demonstrates electrostatic interaction between the negatively charged nanoparticles in the subphase and the positively charged PANI at the air-water interface, which assists the nanocomposite film deposition onto a solid support. To enhance the film's

* Corresponding author.
E-mail address: marshaldhayal@yahoo.com (M. Dhayal).

https://doi.org/10.1016/j.apsadv.2022.100264
Received 25 December 2021; Received in revised form 12 May 2022; Accepted 25 May 2022
Available online 6 June 2022

conductivity, conductive polymer (polyaniline) has been used as a potential candidate due to its low cost, flexible modification, and easy synthesis [26]. The other advantage of polyaniline (PANI) is having a reactive -NH- group in the polymer chain, imparting the system's hydrophilic character. However, PANI suffers from a few limitations, mainly stability and low processing ability which had been addressed in ample research by doping with various nanoparticles [27–30]. In this study, titanium dioxide (TiO_2) nanoparticles were doped in aniline, and the electrochemical polymerization process was used for synthesizing PANI-TiO_2 nanocomposites. Many methods have been used to synthesize PANI-TiO_2 nanocomposites, such as oxidative chemical polymerization of aniline in the presence of TiO_2, polymerization, and physical mixing [31–33]. However, all these methods do not provide control over depositing a single molecular layer; hence the responses are as bulk properties, without precision control over molecular layers and thickness of the films. Thus, appropriate conditions were optimized to prepare low-density dispersions of PANI-TiO_2 in suitable solvents for the deposition of polyaniline-TiO_2 nanocomposite thin films by the Langmuir-Blodgett process.

This study introduced a scheme in which PANI-TiO_2 nanocomposites were synthesized by electropolymerization [34] of a mixture of aniline and TiO_2 nanoparticles on an ITO substrate. Further, the electropolymerized PANI-TiO_2 nanocomposites were dissolved in a solution of N-methyl-2-pyrrolidone (NMP) and isopropanol for monolayer deposition through the LB process. This may provide an advantage in increased conductivity of nanocomposites, higher charge transfer on the electrode surface, and uniform functionalization sites for binding antibodies. X-ray photoelectron microscopy (XPS), scanning electron microscopy (SEM), and transmission electron microscopy (TEM) were used to characterize the physico-chemical properties of PANI-TiO2 nanocomposites and LB-monolayer. Cyclic voltammetry and differential pulse voltammetry measurements were performed to measure the redox current of LB films of PANI-TiO_2. The prepared LB film of PANI-TiO_2 was functionalized by immobilizing monoclonal anti-glutamate antibodies and used to detect MSG through an electrochemical process. MSG is a naturally occurring non-essential amino acid commonly used in the food industries to enhance the flavor of food products [35].

2. Experimental section

2.1. Materials

Isopropanol, L-glutamic acid monosodium salt hydrate 99% (MSG), N-(3 dimethylamino propyl)-N′-ethyl carbodiimide hydrochloride (EDC), N-hydroxysuccinimide (NHS), sodium phosphate monobasic (NaH_2PO4), disodium hydrogen phosphate (Na_2HPO_4), potassium chloride (KCl), sodium hydroxide (NaOH), sulfuric acid, hydrogen peroxide, ammonia, N-methyl-2-pyrrolidone (NMP), ITO coated glass, titanium isopropoxide, nitric acid and potassium ferrocyanide [$K_4Fe(CN)_6$] were purchased from Sigma-Aldrich. Bovine Serum Albumin (BSA) was procured from AcRos. Rabbit Anti-glutamate antibody was obtained from Merck Millipore, USA. Deionized (DI) water from a Millipore system (~18.2 MΩ cm) was used to prepare experimental solutions.

2.2. Preparation of TiO_2 nanoparticles

TiO_2 nanoparticles were synthesized by the sol-gel method using titanium isopropoxide, isopropanol, and nitric acid in a quantity of 7.4 ml, 91.1 ml, and 1.5 ml, respectively, and were mixed under strong magnetic stirring. Then the solution was stirred at a temperature of 60 °C for one h, which led to the formation of white powder, which was heated to 450 °C in the ambient atmosphere to improve the crystalline nature.

2.3. Preparation of polyaniline-TiO_2 nanocomposite

The electropolymerization of the aniline monomer was carried out in a three-electrode cell. ITO coated glass was used as the working electrode, a platinum wire as the auxiliary electrode, and Ag/AgCl as a reference electrode. For the electrochemical polymerization, a solution of 500 μl of sulfuric acid and 91 μl of aniline in 10 ml DI was used. Further, 100 mg TiO_2 was added to this prepared solution and sonicated for 30 min. Electro-polymerization was achieved by sweeping the potentials from −0.3 V to 0.9 V for 21 cycles with a sweep rate of 30 mV s^{-1} and continuous purging of 99% pure nitrogen gas. The PANI-TiO_2 nanocomposites were collected by physical removal from the ITO substrate.

2.4. Preparation of LB film on ITO glass

ITO glass was cleaned in a solution of hydrogen peroxide, ammonia, and DI water in the ratio of 1:1:5 at 75 °C for 30 min and then rinsed with ethanol and dried with the help of 99% pure nitrogen. The trough (mini-trough (KSV-NIMA, Finland) was cleaned with ethanol, followed by DI, and was dried using nitrogen gas to obtain a contamination-free subphase for monolayer.

To prepare LB film of PANI-TiO_2 nanocomposite, 1 mg/mL PANI-TiO_2 nanocomposite was dissolved in a solution of NMP and isopropanol in a ratio of 1:9 and was probe sonicated for 30 min. Then 200 μL of this solution was spread using a Hamilton microsyringe over the trough, containing ultrapure Milli-Q (pH 6.00) water. NMP having a higher density than Milli-Q water, got settled at the bottom of the trough while isopropanol, being volatile, left the system [36]. After approximately 30 min, the composite material remained on the water surface. Then the cleaned ITO substrate was clamped to the dipper, and barriers were compressed at a speed of 10 mm min^{-1} to dense the nanocomposite layer on the water surface. LB films were deposited on substrates using the vertical dipping at a rate of 2 mm min^{-1}. The depositions were made at a constant pressure of 10 mN m^{-1} and the deposited film was dried in a vacuum desiccator overnight.

2.5. Instrumentation

Electrochemical measurements were performed using GAMRY Reference 3000, potentiostat/ galvanostat/ZRA, USA. A transmission electron microscope (JEOL JEMCX11, Japan) at an operating voltage of 150 kV was used to check the deposited film's surface characteristics. The samples were prepared after drop-casting the diluted solution over the carbon-coated copper grid with 400 mesh. Field emission scanning electron microscopy (FESEM) (Zeiss sigma VP FE-SEM, Germany) and XPS (ESCLAB Xi+, Thermo-fisher Scientific) were used for surface morphology and elemental quantifications, respectively. LB film was deposited using a mini-trough (KSV-NIMA, Finland). X-ray diffraction (XRD) patterns were taken by Rigaku mini Flex-600 X-ray diffractometer with Cu Kα radiation (λ=1.5418 Å). The scan was carried out at a 2°/min speed and a 2θ range from 10° to 80°. The UV–visible spectral measurements were carried out using the Shimadzu UV-visible spectrophotometer (Tokyo, Japan).

2.6. Preparation of amperometry mono sodium glutamate (MSG) biosensor

The following optimized procedure was used for the preparation of the glutamate biosensor. Firstly, the LB films of PANI-TIO_2 nanocomposite were deposited onto the ITO coated glass and dried overnight at room temperature. 100 mM NHS and 400 mM EDC were prepared as stock solutions in 100 mM PBS and stored at 4°C. 10 μL of anti-glutamate monoclonal antibodies (1:100 dilution in PBS) were immobilized onto the functionalized electrode and kept undisturbed for 12 h at 4 °C. The surface was rinsed thoroughly with PBS to remove the unbound

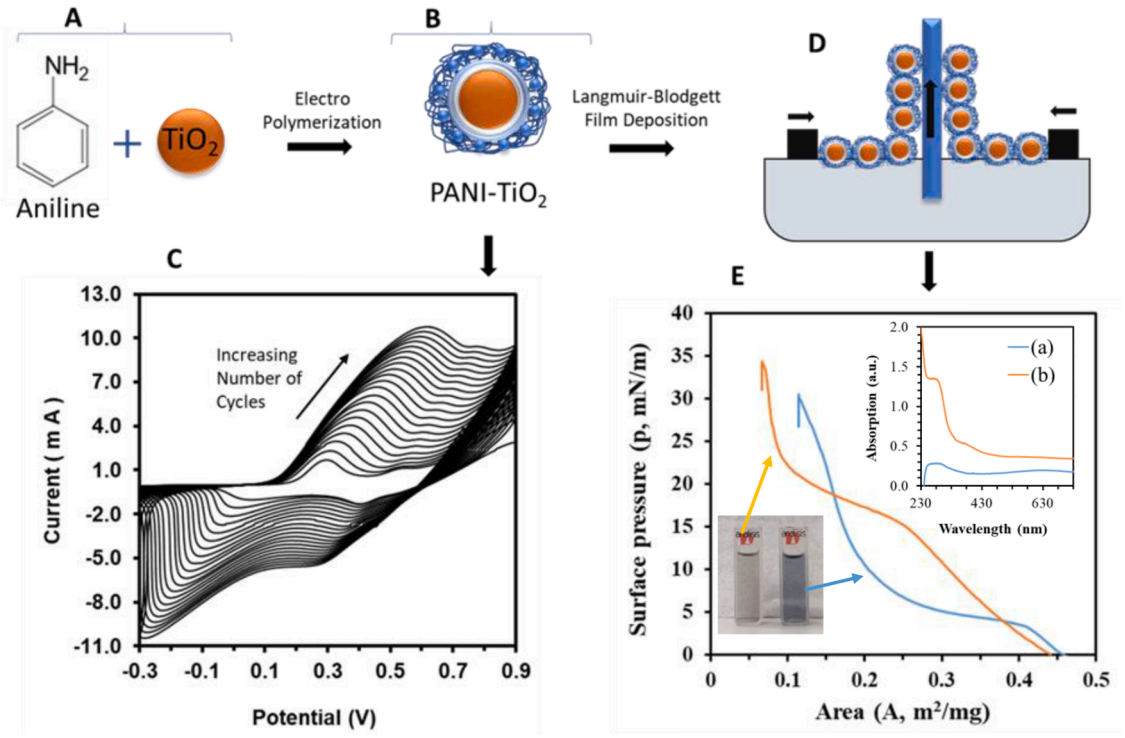

Fig. 1. (A) Schematic representation of electrochemical polymerization of aniline and TiO_2. (B) Diagrammatic illustration of PANI-TiO_2 nanocomposites, (C) CV response of electrochemical polymerizing PANI-TiO_2 for successive 21 cycles, (D) Schematic illustration of L-B film deposition of PANI-TiO_2, and (E) Surface pressure - area (p-A) curve during optimizing of LB film deposition conditions where (a) PANI and (b) PANI-TiO_2; inset images shows UV–vis spectra of (a) PANI and (b) PANI-TiO_2 along with optical images of their suspension in a solvent.

antibodies. Further, 50 μL of BSA was added onto the surface to block non-binding sites at the surface. The freshly prepared functionalized surface of PANI-TiO_2 was used for amperometry experiments.

3. Result and discussion

Electropolymerisation of TiO_2 nanoparticle-containing protonated aniline was done in the acidic pH using a three-electrode system on ITO electrodes, as shown in the schematic representation in Fig. 1(A, B). The polymerization reaction was performed by applying voltage from −0.3 V to 0.9 V in each cycle for successive 21 cycles. The cyclic voltammetry response of each cycle during electrochemical polymerization was recorded, and the results are shown in Fig. 1C. A fine powder of PANI-TiO_2 was collected from the ITO surface after the completion of electropolymerization and dissolved. Both PANI and PANI-TiO_2 nanocomposite began a homogenous and stable dispersion in NMP and isopropanol. The relatively low density of the homogenous solution enabled the preparation of a floating nanocomposite monolayer on the water as a steady air-water interface. UV–vis spectra of PANI and PANI-TiO_2 in NMP solvent were obtained for the solutions used for L-B film deposition (Fig. 1D), and the results are shown inset of Fig. 1E along with their optical images. Separately, the PANI and PANI-TiO_2 solutions were gently dispersed on the water interface, and the pressure-area (p-A) isotherms were recorded during the PANI-TiO_2 Langmuir monolayer formation at the water-air interface (Fig. 1E). The water surface available area in these isotherms was measured in m^2 with the dispersed quantities of PANI and PANI-TiO_2 in mg^{-1}. The PANI-TiO_2 isotherm showed a reduction in surface area from 0.45 to 0.24 m^2/mg, resulting in a linear increase in the pressure from 0 to 15 mN/m, whereas a further decrease in the area showed a transition in the rate of change in the surface pressure. This indicated a shift from a single layer to a multilayer of the molecules. Thus, for depositing LB film of PANI-TiO_2, 10 mN/m pressure was chosen. During this transition, the nanosheets of PANI-TiO_2 float on water due to the surface tension making a steady water-air interface [37]. For transferring water-air interface LB films of PANI-TiO_2 on the ITO electrode, chemically pretreated ITO substrate was clamped to the dipper, and films were deposited on substrates using the vertical dipping at a speed of 2 mm min^{-1}, as schematically shown in Fig. 1D.

The PANI-TiO_2 nanocomposite solution used to prepare LB film was drop cast on a copper TEM grid, and TEM images of the films were acquired and results are shown in Fig. 2A. A high-resolution TEM image was acquired for individual single particles of TiO_2, and a systematic titania atomic arrangement was observed having an interatomic distance of ~ 0.35 nm, corresponding to the anatase (101) crystalline plane (Fig. 2B). The presence of TiO_2 has further confirmed with energy dispersive analysis at the same spot where the TEM analysis was performed (Fig. 2C). A peak corresponding to TiO_2 was obtained in the EDX pattern. This confirmed the presence of TiO_2 in the PANI-TiO_2 nanocomposite. A uniform distribution of TiO_2 was observed with an average size of ~ 5 nm calculated by J-image analysis, as shown in the bar graph of particles size distribution in Fig. 2D.

The X-ray diffraction pattern of PANI, TiO_2, and PANI-TiO_2 films on glass substrates was analyzed by an X-ray diffractometer, and the results are shown in Fig. 2E. The XRD pattern of PANI shows peaks corresponding to crystallite structures associated with (100) and (110) planes [JCPDS No. 53–1718]. The XRD pattern of TiO_2 shows distinct well defined peaks that could be indexed to tetragonal structure with anatase phase. XRD peaks of TiO_2 film were observed at 24.7°, 37.46°,47.36°,54.00°, and 62.08°, corresponding to crystal planes (101), (004), (200), (105), and (204), respectively [36,38]. All these positions of TiO_2 peak in XRD spectra were attributed to the anatase structure of TiO_2 (JCPDS-73/1764). The XRD pattern of PANI-TiO_2 shows distinct well-defined peaks that could be indexed to tetragonal structure with anatase phase. The background glass amorphous characteristics dominated the XRD peak for the condition; however, a small peak in the XRD pattern of TiO_2 film was observed at 24.7°, which corresponds to crystal planes (101) of the anatases phase. Compared to TiO_2, the PANI- TiO_2 diffraction peaks were revealed to broaden and

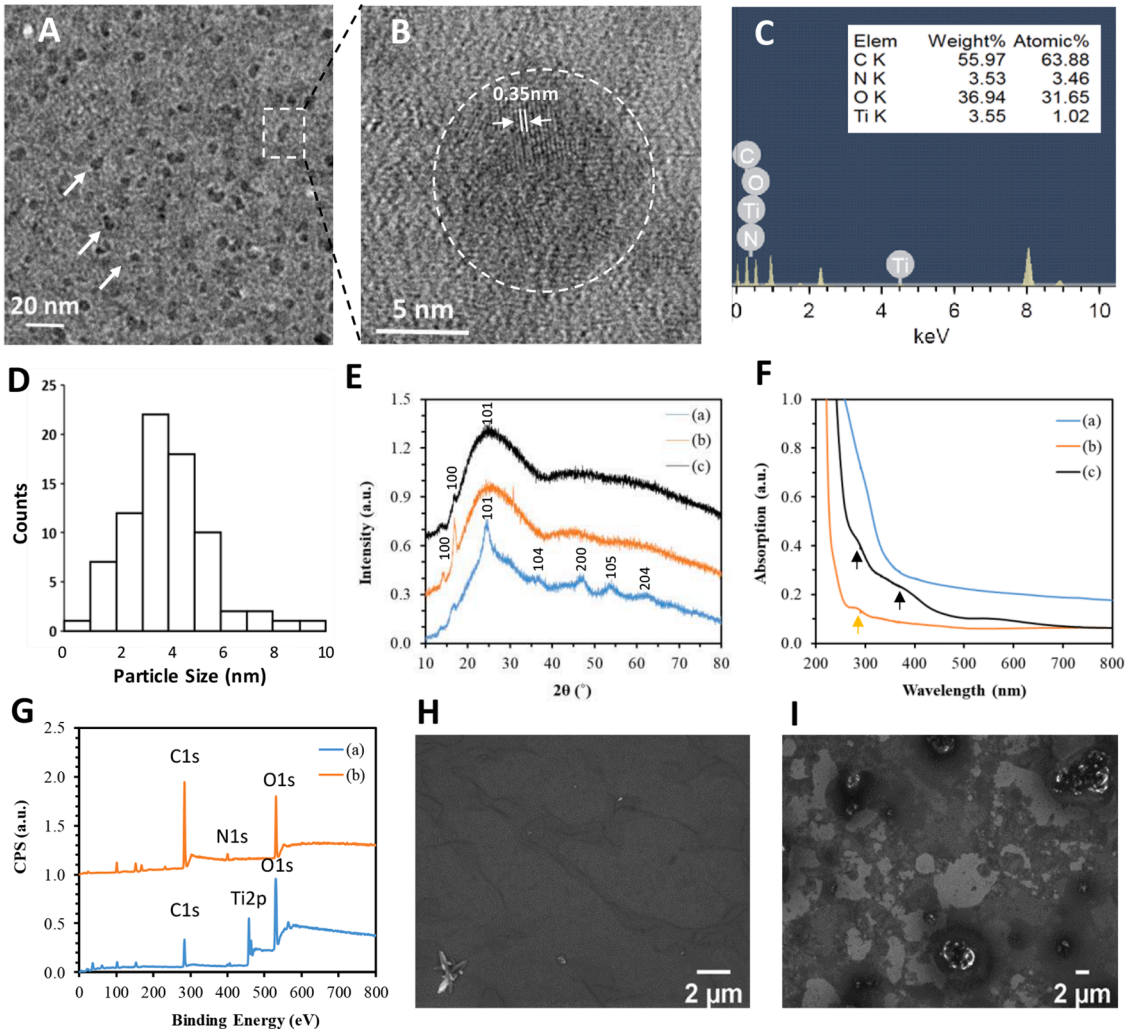

Fig. 2. (A) TEM image of PANI-TiO_2, (B) High-resolution TEM images showing lattic pattern of TiO_2, (C) Energy dispersive X-ray analysis of PANI-TiO_2 nanocomposites showing the relative atomic proportion of different elements present in nanocomposites, (D) bar graph of TiO_2 nanoparticle size distribution in PANI-TiO_2. (E) XRD pattern of (a) TiO_2, (b) PANI and (c) PANI-TiO_2, (F) UV–vis spectra of (a) TiO_2, (b) PANI and (c) PANI-TiO_2, (G) Wide scan X-ray photoelectron spectra of TiO_2 and PANI-TiO_2 film surface, (H) SEM image of PANI-TiO_2 LB film and (I) SEM image of immunosensor with BSA passivation after antibody functionalization on PANI-TiO_2 LB film.

decrease the intensity, and this may be due to the polymerization of PANI onto the TiO_2 in the composites [39].

Fig. 2F shows the UV–Vis absorbance spectra of TiO_2, PANI, and PANI-TiO_2 composites. The spectral optical absorption peak was at 290 nm for PANI, peak at 320 nm for TiO_2, and peaks at 290 nm and 380 nm for PANI-TiO_2 nanocomposites. This could be attributed to the π–π* and polaron–π* transition in the conducting PANI [39,40] The absorption edge was shifted towards the longer wavelength side for PANI-TiO_2 nanocomposite might be due to coordinate complex formation between TiO_2 nanoparticles and PANI [41].

The PANI-TiO_2 LB film deposited on the ITO substrate was further characterized by X-ray photoelectron spectroscopy [42], and the results are shown in Fig. 2G. A broad scan XPS spectrum of TiO_2 nanoparticles and PANI-TiO_2 LB film was obtained. XPS elemental analysis of PANI-TiO_2 showed 73%, 21.9%, 4.7%, and 0.5% atomic percentage proportions of carbon, oxygen, nitrogen, and titanium, respectively, as shown in the figure. Relative proportions of different elements at the surface were calculated from these spectra. The ratio of Ti/O at the surface of TiO_2 nanoparticles in XPS broad spectra was 0.24. This O/Ti ratio was decreased in PANI-TiO_2, and the appearance of the peak corresponding to nitrogen is shown in the XPS wide scan spectra. This confirmed the aniline polymerization on the surface of TiO_2. SEM image of LB films of PANI-TiO_2 on ITO electrode before and after immobilization of monoclonal anti-glutamate antibodies is shown in Fig. 2 (H, I). SEM image of the film surface showed a topological view and confirmed the formation of uniform structures of PANI-TiO_2 across the surface, and after immobilization of antibodies, a change in surface topography indicated functionalization of the surface.

The electrochemical response of the ITO, LB film of PANI-TiO_2 on ITO, and antibody immobilized LB film of PANI-TiO_2 on ITO as the working electrode and BSA passivated antibodies immobilized PANI-TiO_2 electrode was assessed in 100 mM PBS containing 5 mM K_4[Fe (CN)$_6$] and 0.1 M KCL (Fig. 3). The potential range from −0.3 V to 0.7 V was used for measurements. Anodic (I_{pa}) and cathodic (I_{pc}) peak currents in cyclic voltammetry response of immunosensor were assessed. I_{pc} and I_{pa} were increased from 318.2 µA to 387.3 µA and 194.5 µA to 221 µA after deposition of LB film of PANI-TiO_2 on ITO. The conductivity enhancement was seen due to conducting nature of PANI-TiO_2, which may have helped in the fast electron transfer process between the electrolyte and the electrode. Further immobilization of antibodies on PANI-TiO_2 reduced both anodic and cathodic peak current from 387.3 µA to 322.5 µA and 221 µA to 182 µA. This may happen due to the non-conductive nature of antibodies; however, even after reduction, it retains peak current values similar to conducting ITO electrodes.

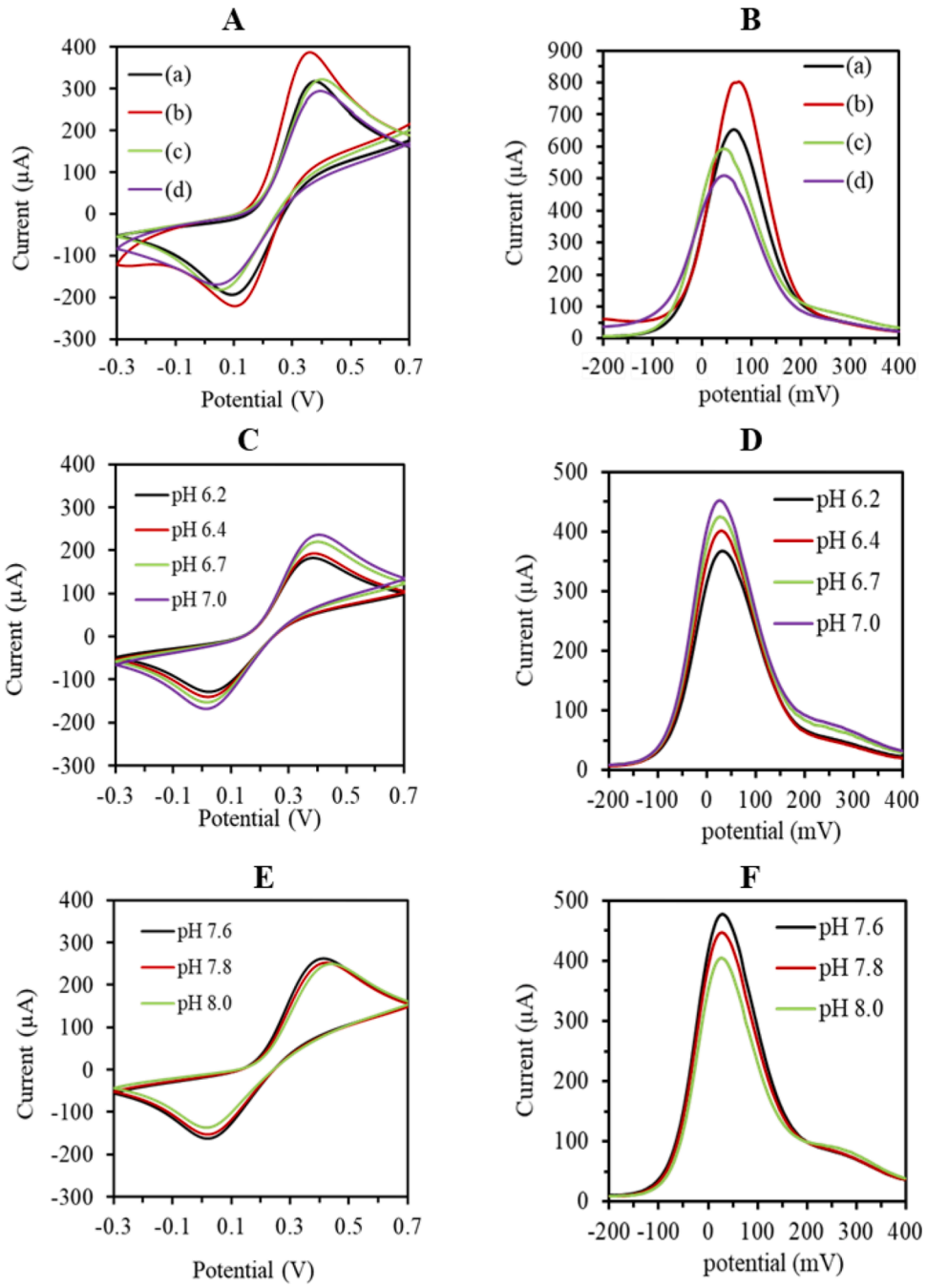

Fig. 3. (A) CV and (B) DPV of different types of working electrodes. (a) ITO electrode, (b) PANI-TiO_2 LB film working electrode, (c) Rabbit anti-glutamate antibodies immobilized PANI-TiO_2 LB film working electrode, and (d) BSA passivated rabbitanti-glutamate antibody immobilized PANI-TiO_2 LB film working electrode. (C) CV and (D) DPV of PANI-TiO_2 immunosensor at various pH in acidic range and (E) CV and (F) DPV of PANI-TiO_2 immunosensor at various pH in basic range.

Electrochemical surface area of electrodes (A) were calculated with the use of Randles-Sevcik equation

$$I_p = 2.69 \times 10^5 A\, C\, D^{1/2} \nu^{1/2} n^{3/2} \quad (1)$$

where I_p = oxidation peak current of K_4 [$Fe(CN)_6$] in ampere obtained from CV of 5 mM $K_4[Fe(CN)_6]$ at the scan rate of 30 mVs^{-1}, A = electrochemical surface area of electrode in cm^2, C = concentration of analyte (5 mM $K_4[Fe(CN)_6]$ in 0.1 M KCL) in mol cm^{-3}, D- Diffusion coefficient of $K_4[Fe(CN)_6] = 6.5 \times 10^{-6}$ cm^2 s^{-1}, ν scan rate in V s^{-1} and 'n' number of electron transfer in the redox reaction ($n = 1$).

The measured electrochemical active area of the electrodes ITO, LB film of PANI-TiO_2, antibody immobilized on PANI-TiO_2 film and after passivation with BSA from the above equation and parameters were ~ 0.54 cm^2, ~ 0.65 cm^2, ~ 0.54 cm^2 and ~ 0.50 cm^2, respectively.

Cathodic ($E_{p,c}$) and anodic peak ($E_{p,a}$) potential were measured by CV response of different electrodes of ITO, PANI-TiO_2, antibodies immobilized PANI-TiO_2 and BSA passivated antibodies immobilized PANI-TiO_2 working electrodes. The difference in the potentials of both anodic and cathodic peaks ($\Delta E_p = E_{p,a} - E_{p,c}$) was calculated for these four different electrodes. The calculated ΔE_p for ITO, PANI-TiO_2, antibodies immobilized PANI-TiO_2, and BSA passivated antibodies immobilized PANI-TiO_2 were 0.29 V, 0.26 V, 0.35 V, and 0.36 V, respectively. The ΔEp remains similar for antibodies immobilized PANI-TiO_2 and BSA passivated antibodies immobilized PANI-TiO_2 electrode whereas PANI-TiO_2 showed a decrease in ΔEp, which confirmed fast kinetics of

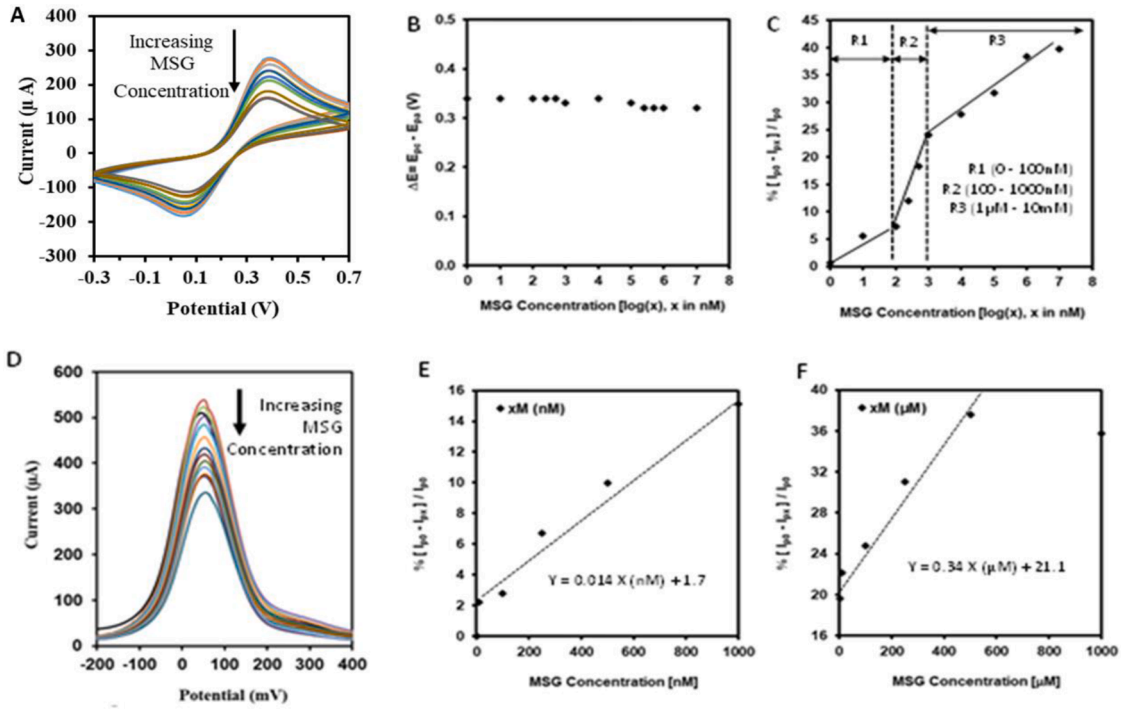

Fig. 4. (A) CV response of PANI-TiO_2 immunosensor working electrode with different concentrations of MSG, (B) Relative change in peak potential with MSG concentrations, (C) Relative change in peak current with MSG concentrations, (D) DPV response of CS-GNP-IgG working electrode with different concentrations of MSG. (E) Relative change in% peak current with MSG concentrations varying in nM concentration, and (F) Relative change in% peak current with MSG concentrations varying in µM concentration.

electron transfer on the electrode surface. Electron transfer (n) on the electrode surface is inversely proportional to ΔE_p (n α 1/ ΔE_p) [43]. About 10% of the decrease in the ΔE_p was observed, and a similar proportion of electrons was expected to increase in the process. This is expected due to the higher conductivity of aniline molecules in PANI and is supported by increased peak currents of both oxidation and reduction processes. Further immobilization of antibodies on the PANI-TiO_2 surface showed an increase in ΔE_p by 35%, resulting in a decrease in a similar proportion of electron transportation. The observations are consistent with expected outcomes as the non-conducting nature of antibodies at the electron's surface reduces its diffusion from the electrolyte to the working electrode surface.

DPV response of ITO and different platforms (PANI-TiO_2, Antibody-PANI-TiO_2, and BSA-antibody-PANI-TiO_2) on ITO electrode was carried out in the same electrolyte. Peak current (I_p) was increased from 654 µA to 804 µA after LB film deposition of PANI-TiO_2 on the ITO electrode. The enhanced conductivity of PANI-TiO_2 may be due to the conductive nature of aniline molecules. Rabbit anti-glutamate antibodies immobilized PANI-TiO_2 surface result showed a decrease of I_p from 804 µA to 594 µA, similar to ITO response. Further passivation of the surface by BSA was achieved to minimize the direct interaction of electrolytes at the working electrode surface.

The antibody immobilized at the surface of PANI-TiO_2 may respond differently to a change in the pH of the electrolyte solution. CV has been recorded on immunosensor working electrodes at pH variation in acidic (pH from 6.2 to 7), and basic (7.6 to 8) ranges, and the results are shown in Fig. 3 (C, E). I_{pc} and I_{pa} were decreased from 236.3 µA to 182.5 µA, and 168 µA to 128.5 µA with the reduction in pH from 7.0 to 6.2 on antibodies immobilized LB film of PANI-TiO_2 on ITO. The ΔE_p was decreased by 8% with a decrease in pH values in the acidic region, indicating an increase in electron transportation. This could be due to the polarization of antibodies' surfaces while the number of charged particles in electrolytes increased with pH reduction from its neutral value. Similar results were observed for the increase in pH in the basic region. I_{pc} and I_{pa} were decreased from 262 µA to 250 µA and 163 µA to 137 µA, respectively, with the increase in pH from 7.6 to 8.0 on antibodies immobilized LB film of PANI-TiO_2 on ITO. The ΔE_p was increased by 7%, increasing pH values in the basic region, indicating a decrease in electron transportation. This observation is consistent with acidic pH variation observations, where a relative increase in the number of electrons on the electrode surface was observed. In contrast, the number of charged particles in electrolytes increased with pH reduction from its neutral value. Whereas with the increase in basic pH, the charge polarity in the electrolyte may be reversed, and a decrease in a similar proportion of charged particles was observed on the electrode surface. The potential of the peak current varies from ~ 0.38 V to ~ 0.44 V by changing pH from 6.2 to 8 as indicated in the results. Using the Nernst equation that shows a linear response in the change in potential with pH variation with a constant term 59 mV/n, which represents the slope of the obtained data and in our observation the calculated value of $n = 2$.

DPV response of BSA-antibody-PANI-TiO_2 on the ITO electrode at various pH levels in acidic and basic conditions was also measured, and the results are shown in Fig. 3 (D, F). Peak current (I_p) was decreased from 453 µA to 368 µA with a decrease in pH from 7 to 6. Similarly, in the basic region, the pH increases from 7.6 to 8, reducing the peak current from 476 µA to 404 µA. The excess concentration of charge in the electrolyte might polarize the antibodies at the surface of the working electrode, hence decreasing the peak current. Therefore, the experimental observations indicated the highest current for the pH range (7.2 to 7.4). This is also a safe range for glutamate, which can be protonated or de-protonated in the acidic and basic conditions wherein glutamate gets converted to glutamic acid. Thus, it could not interact with the antibody [44]. While in basic condition, hydroxyl ion as cationic sites on the functionalized electrode surface results in interference which causes a change in potential.

The interaction of the BSA passivated antibody immobilized PANI-TiO_2 on the ITO working electrode at different MSG concentrations was assessed. Gradually the MSG concentration was increased, and at every step, CV response was recorded, and results are shown in Fig. 4A. The ΔE_p remains constant with increasing concentration of MSG. Anodic

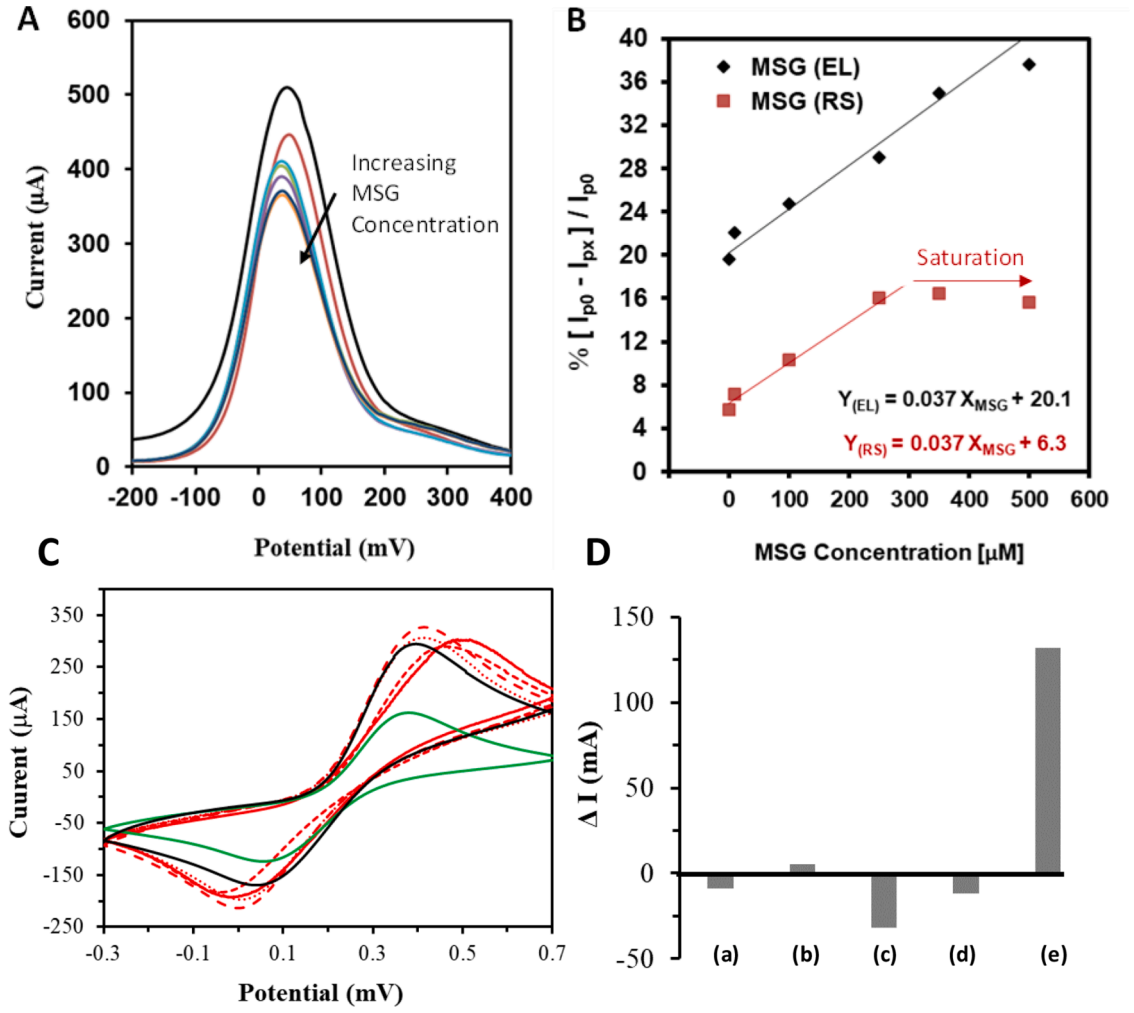

Fig. 5. (A) DPV response of PANI-TiO_2 immunosensor working electrode without and with tomato sauce at different concentrations of MSG, (B) Immunosensor response for quantification of MSG concentrations where MSG (EL) represents MSG in standard electrolyte and MSG (RS) represents MSG in tomato sauce. (C) CV response of immunosensor with different analytes, (CV response of black- immunosensors, green- with MSG and red- with different analytes) and (D) Relative change in peak current of CV response while different analytes added into the electrolyte, (a) ascorbic acid, (b) arginine (c) aspartic acid (d) cysteine and (e) MSG.

(I_{pa}) and cathodic (I_{ca}) peak currents response of working electrodes with and without MSG in electrolytes were assessed and compared. The value of Ipa was measured, and the% relative change [$(I_{po} - I_{px})/I_{po}$], where I_{po} is peak current without MSG and I_{px} is peak current at 'x' nM of MSG, was plotted with a wide range of MSG variation in the electrolyte. Initially, at a scarce concentration of MSG (R1 = 0 to 100 nM) straight-line response was observed; the second response was for R2 from 100 nM to 1000 nM, and finally, the third region, R3, from 1 μM to 10 mM. The results suggested that with precise control of surface molecular layer properties, a wide range of MSG detection was possible with different calibration regions.

DPV results in Fig. 4 revealed that peak current is inversely proportional to the increase in MSG concentration. This may be due to the formation of anti-glutamate antibodies and L-glutamate antigen complex, which plays an important role in the selective detection of MSG [45]. This complex system creates a diffusion layer that blocks the transfer of ions between the solution and electrode surface. As a result, active sites for electron transfer were reduced, and the working electrode platform's conductivity was decreased with an increase in MSG concentration. The% relative change in peak current with MSG concentration was also consistent with CV measurement, as shown in Fig. 4C. The working electrode developed with PANI-TiO_2 showed enhancement in the charge transportation, whereas functional group presence allowed effective immobilization of antibodies at the surface. The antibodies immobilized electrode showed exquisite sensitivity for detecting MSG in the range of nM to mM.

DPV was used to obtain current-voltage characteristics of immunosensor prepared using PANI-TiO_2 LB films at different concentrations of MSG added in tomato sauce, and the relative change in peak current was recorded. DPV measurements were carried out by placing antibodies-immobilized working electrodes in 10 ml of phosphate buffer (pH 7.0), having MSG added tomato sauce. The solution was stirred for 30 s before taking each measurement. The MSG concentrations in tomato sauce were increased by adding MSG with gradual increments in the range of 10 μM to 500 μM in buffer solution, and the results are shown in Fig. 5A. Platinum wire and Ag/AgCl were used as counter and reference electrodes, respectively. Fig. 5B showed a quantitative analysis of MSG detection in terms of percentage relative changes $\Delta I = [100\{(I_{PO} - I_{PX})/I_{PO}\}]$ in peak current for PANI-TiO_2 electrode. I_{PO} and I_{PX} are peak current measured in DPV without the use of MSG and with 'X' molar concentration of MSG, respectively. Linear response for detecting MSG was observed, which was expressed as $\Delta I_{RS} = 0.037\ X_{MSG} + 6.3$, where X_{MSG} is the concentration of MSG in tomato sauce (described as a real sample) added to electrolyte during the measurement. The detection sensitivity was calculated from the linear response slope in current variation with increasing MSG concentrations, which was 37 mA/nM. The detection range for the real sample tested was from 1 μM to 250 μM concentration. A quantitative analysis of MSG detection in terms of

Table 1
Relative comparison of different types of biosensors for detection of MSG.

Immobilization Technique	Refs.	Lowest Detection	Sensitivity	Linear Range
Au@MoS2/chitosan electrode using monoclonal antibody	[38]	0.05 μM	NA	0.05 to 200 μM
Au@ chitosan electrode using monoclonal antibody	[39]	0.11nM	NA	0.1 nM to 1μM
Titania and ceria and nanoparticles for glutamate detection in hypoxic environments	[46]	0.594μM	0.79 nA/μM	5 – 50μM
Carboxylated MWCNT/gold nanoparticles/chitosan composite film modified Au electrode	[47]	1.6μM	155 nA/ μM/cm^2	5 – 500 μM
Polypyrrole nanoparticles/ polyaniline modified Au electrode	[48]	0.1nM	533 nA/ μM/cm^2	0.02 - 400μm
Immobilization of GLDH with Chitosan, drop coated onto a screen-printed carbon electrode	[49]	1.5 μM	0.44 nA/μM	12.5 - 150μM
Immobilization of NAD^+ and GLDH by using a mixture CHIT/MWCNT/MB drop coated onto screen-printed carbon electrode	[50]	3μM	0.39 nA/μM	7.5 - 105μM

percentage relative changes $\Delta I = [100\{(I_{PO} - I_{PX})/I_{PO}\}]$ in peak current for PANI-TiO_2 electrode was also calculated for the use of MSG in the standard electrolyte from the DPV measurements, as shown in Fig. 4D. These were described as MSG in the electrolyte MSG (EL). I_{PO} and I_{PX} are peak currents measured in DPV without using MSG and with 'X' molar concentration of MSG, respectively, by adding MSG to the standard electrolyte. Linear response for detecting MSG was observed, which was expressed as $\Delta I_{EL} = 0.037\ X_{MSG} + 20.1$, where X_{MSG} was the concentration of MSG in the standard electrolyte (described as electrolyte) during the measurement.

The detection sensitivity was calculated from the linear response slope in current variation with increasing MSG concentrations, which was 37 mA/nM. The range of detection of MSG was tested in the standard electrolyte from 1 μM to 500 μM concentration. The detection sensitivity remained unchanged for both tomato sauce samples and standard electrolytes. However, the detection range for MSG in standard electrolytes showed linear response for an extended range, whereas real samples showed saturation at 250 μM MSG concentration in the current study. The working electrode developed with PANI-TiO_2 showed enhancement in the charge transportation, whereas functional group presence allowed effective immobilization of antibodies at the surface. The antibodies immobilized electrode showed exquisite sensitivity and consistency for detection of MSG. Table 1 summarizes the detection sensitivity of MSG obtained with different types of biosensors platforms prepared by different methods.

The specificity of the developed biosensor was also examined with the use of other analytes (ascorbic acid, arginine, aspartic acid, cysteine) in the electrolytes. Fig. 5C shows the CV response of the biosensor platform with the use of similar molar concentrations of their in the electrolyte. It is clearly evident that there has not been a significant change in the peak current of CV response acquired with the use of different analytes. The addition of a similar molar concentration of MSG in the electrolyte had substantially reduced the peak current in CV response. Relative change in the oxidation peak current during measuring CV response was calculated for all different analytes and results are plotted in Fig. 5D. These results confirmed the advantage of using nanocomposites having both biocompatible and conducting nature for making biosensors platforms by depositing monolayers for effectively quantifying analytes in the electrolyte with higher sensitivity and selectively.

4. Conclusion

The electropolymerization of aniline monomer with TiO_2 was carried out using cyclic voltammetry, and a fine powder of PANI-TiO_2 nanocomposites having an average diameterter of 5 nm was obtained. LB monolayer of these nanocomposites was prepared on ITO coated glass electrode. FE-SEM, TEM, and XPS confirmed the presence of TiO_2 in PANI-TiO_2 nanocomposite and their LB coating. Further monoclonal antibodies specific to L-glutamic acid were immobilized onto the LB film through an EDC—NHS coupling reaction. The antibodies immobilized electrodes were successively used to quantify MSG ranging from 1 nM to 500 μM in the standard electrolyte. A linear relationship was obtained between the change in current and the concentration of MSG.

Declaration of Competing Interest

The authors declare that they have no known competing financial interests or personal relationships that could have influenced the work reported in this paper.

Acknowledgment

The authors acknowledge financial support from the Department of Biotechnology (Govt. of India) grant number BT/PR16223/NER/95/494/2016 and Central Instrument Facility, Indian Institute of Technology (BHU) Varanasi, for providing Transmission Electron Microscopy. Devdutt Sharma thanks Juhi Jaiswal, Ashish Singh, and Shubhangi for proofreading the manuscript.

Reference

[1] I.H. Cho, D.H. Kim, S. Park, Electrochemical biosensors: perspective on functional nanomaterials for on-site analysis, Biomater. Res. 24 (2020) 1–12, https://doi.org/10.1186/s40824-019-0181-y.
[2] M.E. Oliveira, B.V. Lopes, J.H.H. Rossato, G.K. Maron, B.B. Gallo, A.B. La Rosa, R. D.C. Balboni, M.L.F. Alves, M.R.A. Ferreira, L. da Silva Pinto, F.R. Conceição, Electrochemical biosensor based on laser-induced graphene for covid-19 diagnosing: rapid and low-cost detection of sars-cov-2 biomarker antibodies, Surfaces 5 (2022) 187–201, https://doi.org/10.3390/surfaces5010012.
[3] J.H. Kim, Y.J. Suh, D. Park, H. Yim, H. Kim, H.J. Kim, D.S. Yoon, K.S. Hwang, Technological advances in electrochemical biosensors for the detection of disease biomarkers, Biomed. Eng. Lett. 11 (2021) 309–334, https://doi.org/10.1007/s13534-021-00204-w.
[4] Y.I. Zhang, L. Zhang, C. Zhou, Review of chemical vapor deposition of graphene and related application, Acc. Chem. Res. 46 (2013) 2329–2339, https://doi.org/10.1021/ar300203n.
[5] U. Helmersson, M. Lattemann, J. Bohlmark, A.P. Ehiasarian, J.T. Gudmundsson, Ionized physical vapor deposition (IPVD): a review of technology and applications, Thin Solid Films 513 (2006) 1–24, https://doi.org/10.1016/j.tsf.2006.03.033.
[6] L.P. Bicelli, B. Bozzini, C. Mele, L. D'Urzo, A review of nanostructural aspects of metal electrodeposition, Int. J. Electrochem. Sci. 3 (2008) 356–408. WOS: 000256383900001.
[7] S.K. Vishwakarma, J. Jaiswal, K.H. Park, C. Lakkireddy, N. Raju, A. Bardia, M. A. Habeeb, S.A. Paspala, A.A. Khan, M. Dhayal, TiO_2 nanoflowers on conducting substrates ameliorate effective transdifferentiation of human hepatic progenitor cells for long-term hyperglycemia reversal in diabetic mice, Adv. Therapeut. 3 (2020), 1900205, https://doi.org/10.1002/adtp.201900205.
[8] J. Jaiswal, M. Dhayal, Mater. Chem. Phys. 243 (2020), 122663.
[9] M. Dhayal, C. So, J.S. Choi, J. Jun, Control of bio-MEMS surface chemical properties in micro fluidic devices for biological applications, J. Nanosci. Nanotechnol. 6 (2006) 3494–3498, https://doi.org/10.1166/jnn.2006.17968.
[10] D. Sharma, N.N.M. Rao, S. Arasaretnam, V. Annadanam, S. Sainath, M. Dhayal, Functionalization of structurally diverse glycopolymers on graphene oxide surfaces and their quantification through fluorescence resonance energy transfer with fluorescein isothiocyanate, Colloid Polym. Sci. 298 (2020) 365–375, https://doi.org/10.1007/s00396-020-04611-w.
[11] T. Abohalkuma, J. Telegdi, Corrosion protection of carbon steel by special phosphonic acid nano-layers, Mater. Corros. 66 (2015) 1382–1390, https://doi.org/10.1002/maco.201508304.
[12] Dave K, N.N.M. Rao, M. Trinadh, B.A. Monisha, A.V.S. Sainath, M. Dhayal, Spectroscopic and electron microscopic analysis of bi-ligand functionalized glycopolymer/FITC–gold nanoparticles, RSC Adv. 6 (2016) 44392–44401, https://doi.org/10.1039/C6RA04273B.
[13] M. Dhayal, D. Ratner, XPS and SPR analysis of glycoarray surface density, Langmuir (2) (2009) 2181–2187.
[14] I. Langmuir, The mechanism of the surface phenomena of flotation, Trans. Faraday Soc. 15 (1920) 62–74, https://doi.org/10.1039/TF9201500062.

[15] K.B. Blodgett, Films built by depositing successive monomolecular layers on a solid surface, J. Am. Chem. Soc. 57 (1935) 1007–1022, https://doi.org/10.1021/ja01309a011.

[16] F.A. Scholl, P.V. Morais, R.C. Gabriel, M.J. Schöning, J.R. Siqueira, L.C. Orcid, O. N. Oliveira Jr, ACS Appl. Mater. Interfaces 9 (36) (2017) 31054–31066.

[17] A. Katsuhiko, Don't forget Langmuir–Blodgett films 2020: interfacial nanoarchitectonics with molecules, materials, and living objects, Langmuir 36 (2020) 7158–7180, https://doi.org/10.1021/acs.langmuir.0c01044.

[18] M.M. Salleh, A.S. Belal, M. Yahaya, Optical gas sensing of hematin Langmuir-Blodgett films, in: Third International Conference on Thin Film Physics and Applications 3175, 1998, pp. 77–81, https://doi.org/10.1117/12.300641.

[19] M. Ferreira, C.A. Olivati, A.M. Machado, A.M. Assaka, J.A. Giacometti, L. Akcelrud, O.N. Oliveira Jr, Langmuir and langmuir-blodgett films of polyfluorenes and their use in polymer light-emitting diodes, J. Polym. Res. 14 (2007) 39–44, https://doi.org/10.1007/s10965-006-9078-2.

[20] M. Clemente-León, H. Soyer, E. Coronado, C. Mingotaud, C.J. Gómez-García, P. Delhaès, Langmuir–Blodgett films of single-molecule nanomagnets, Angew. Chem. 37 (1998) 2842–2845, https://doi.org/10.1002/(SICI)1521-3773(19981102)37:20<2842::AID−ANIE2842>3.0.CO;2-B.

[21] Z. Matharu, G. Sumana, S.K. Arya, S.P. Singh, V. Gupta, B.D. Malhotra, Polyaniline Langmuir− Blodgett film based cholesterol biosensor, Langmuir 23 (2007) 13188–13192, https://doi.org/10.1021/la702123a.

[22] M. Poonia, V. Manjuladevi, R.K. Gupta, S.K. Gupta, J. Singh, P.B. Agarwal, J. Akhtar, Ultrathin films of single-walled carbon nanotubes: a potential methane gas sensor, Sci. Adv. Mater. 7 (2014) 455–462, https://doi.org/10.1166/sam.2015.1989.

[23] S. Paul, C. Pearson, A. Molloy, M.A. Cousins, M. Green, S. Kolliopoulou, P. Dimitrakis, P. Normand, D. Tsoukalas, M.C. Petty, Langmuir−Blodgett film deposition of metallic nanoparticles and their application to electronic memory structures, Nano Lett. 3 (2003) 533–536, https://doi.org/10.1021/nl034008t.

[24] G. Tanami, V. Gutkin, D. Mandler, Thin nanocomposite films of polyaniline/Au nanoparticles by the Langmuir− Blodgett technique, Langmuir 26 (2010) 4239–4245, https://doi.org/10.1021/la903284g.

[25] Z. Matharu, P. Daggumati, L. Wang, T.S. Dorofeeva, Z. Li, E. Seker, Nanoporous-gold-based electrode morphology libraries for investigating structure–property relationships in nucleic acid based electrochemical biosensors, ACS Appl. Mater. Interfaces 9 (2017) 12959–12966, https://doi.org/10.1021/acsami.6b15212.

[26] S. Ramanavicius, A. Ramanavicius, Conducting polymers in the design of biosensors and biofuel cells, *Polymers (Basel)* 13 (1) (2020) 49, https://doi.org/10.3390/polym13010049.

[27] L. Li, M. Wu, Y. Feng, F. Zhao, B. Zeng, Doping of three-dimensional porous carbon nanotube-graphene-ionic liquid composite into polyaniline for the headspace solid-phase microextraction and gas chromatography determination of alcohols, Anal. Chim. Acta 948 (2016) 48–54, https://doi.org/10.1016/j.aca.2016.11.020.

[28] M. Turemis, D. Zappi, M.T. Giardi, G. Basile, A. Ramanaviciene, A. Kapralovs, A. Ramanavicius, R. Viter, ZnO/polyaniline composite based photoluminescence sensor for the determination of acetic acid vapor, Talanta 211 (2020), 120658, https://doi.org/10.1016/j.talanta.2019.120658.

[29] S. Rani, M.Kamaraj Mangisetti, S. Ramaprabhu, N-doped 3D porous carbon-graphene/polyaniline hybrid and N-doped porous carbon coated gC3N4 nanosheets for excellent energy density asymmetric supercapacitors, Electrochim. Acta 305 (2019) 264–277, https://doi.org/10.1016/j.electacta.2019.03.043.

[30] T.P. Tsele, A. S.Adekunle, O.E. Fayemi, E.E. Ebenso, Electrochemical detection of epinephrine using polyaniline nanocomposite films doped with TiO_2 and RuO_2 nanoparticles on multi-walled carbon nanotube, Electrochim. Acta 243 (2017) 331–348, https://doi.org/10.1016/j.electacta.2017.05.031.

[31] K. Choudhary, V. Manjuladevi, R.K. Gupta, P. Bhattacharyya, A. Hazra, S. Kumar, Ultrathin films of TiO_2 nanoparticles at interfaces, Langmuir 31 (2015) 1385–1392, https://doi.org/10.1021/la503514p.

[32] S. Abaci, B. Nessark, F. Riahi, Preparation and characterization of polyaniline+ TiO_2 composite films, Ionics 10 (2014) 1693–1702, https://doi.org/10.1007/s11581-014-1129-9.

[33] A. Popov, B. Brasiunas, A. Damaskaite, I. Plikusiene, A. Ramanavicius, Electrodeposited gold nanostructures for the enhancement of electrochromic properties of PANI–PEDOT film deposited on transparent electrode, *Polymers (Basel)* 12 (2020) 2778, https://doi.org/10.3390/polym12122778.

[34] S. Ramanavicius, A. Ramanavicius, Charge transfer and biocompatibility aspects in conducting polymer-based enzymatic biosensors and biofuel cells, Nanomaterials 11 (2021) 371, https://doi.org/10.3390/nano11020371.

[35] V. Stoeger, K.I. Liszt, B. Lieder, M. Wendelin, M. Zopun, J. Hans, J.P. Ley, G. E. Krammer, V. Somoza, Identification of bitter-taste intensity and molecular weight as amino acid determinants for the stimulating mechanisms of gastric acid secretion in human parietal cells in culture, J. Agric. Food Chem. 66 (2018) 6762–6771, https://doi.org/10.1021/acs.jafc.8b01802.

[36] G.K. Bhullar, R. Kaur, K.K. Raina, Alignment of polymer dispersed nanometric films of ferroelectric liquid crystalline molecules, J. Appl. Polym. Sci. 41386 (2015) 1–7, https://doi.org/10.1016/j.molliq.2019.111664.

[37] S. Solanki, A. Soni, M.K. Pandey, A. Biradar, G. Sumana, Langmuir–Blodgett nanoassemblies of the MoS2–Au composite at the air–water interface for dengue detection, ACS Appl. Mater. Interfaces 10 (2018) 3020–3028, https://doi.org/10.1021/acsami.7b14391.

[38] R.G. Toro, M. Diab, T.de Caro, M. Al-Shemy, A. Adel, D. Caschera, Study of the effect of titanium dioxide hydrosol on the photocatalytic and mechanical properties of paper sheets, Materials 13 (2020) 1326, https://doi.org/10.3390/ma13061326.

[39] M. Sasikumar, N.P. Subiramaniyam, Microstructure, electrical and humidity sensing properties of TiO_2/polyaniline nanocomposite films prepared by sol–gel spin coating technique, J. Mater. Sci. Mater. Electron. 29 (2018) 7099–7106, https://doi.org/10.1007/s10854-018-8697-9.

[40] S.M. Gupta, M. Tripathi, A review of TiO_2 nanoparticles, Chin. Sci. Bull. 56 (2011) 1639–1657, https://doi.org/10.1007/s11434-011-4476-1.

[41] M.R. Nabid, M. Golbabaee, A.B. Moghaddam, R. Dinarvand, R. Sedghi, Polyaniline/TiO_2 nanocomposite: enzymatic synthesis and electrochemical properties, Int. J. Electrochem. Sci. 3 (2008) 1117–1126.

[42] J. Jun, M. Dhayal, J.H. Shin, J.C. Kim, N. Getoff;, Surface properties and photoactivity of TiO_2 treated with electron beam, Radiat. Phys. Chem. 75 (2006) 583–589, https://doi.org/10.1016/j.radphyschem.2005.10.015.

[43] R. Khan, M. Dhayal, Electrochemical studies of novel chitosan/TiO_2 bioactive electrode for biosensing application, Electrochem. Commun. 10 (2008) 263–267, https://doi.org/10.1016/j.elecom.2007.12.001.

[44] R. Devi, S. Gogoi, S. Barua, H.S. Dutta, M. Bordoloi, R. Khan, Electrochemical detection of monosodium glutamate in foodstuffs based on Au@ MoS2/chitosan modified glassy carbon electrode, Food Chem. 276 (2019) 350–357, https://doi.org/10.1016/j.foodchem.2018.10.024.

[45] D. Sharma, R. Devi, J. Jaiswal, H.S. Dutta, R. Khan, M. Dhayal, A highly sensitive immunosensor based on in situ reduced gold-chitosan nanocomposite for detection of monosodium L-glutamate, J. Biosyst. Eng. 47 (2022) 28–38, https://doi.org/10.1007/s42853-022-00127-z.

[46] R.E. Özel, C. Ispas, M. Ganesana, J.C. Leiter, S. Andreescu, Glutamate oxidase biosensor based on mixed ceria and titania nanoparticles for the detection of glutamate in hypoxic environments, Biosens. Bioelectron. 52 (2014) 397–402, https://doi.org/10.1016/j.bios.2013.08.054.

[47] B. Batra, C.S. Pundir, An amperometric glutamate biosensor based on immobilization of glutamate oxidase onto carboxylated multiwalled carbon nanotubes/gold nanoparticles/chitosan composite film modified Au electrode, Biosens. Bioelectron. 47 (2013) 496–501, https://doi.org/10.1016/j.bios.2013.03.063.

[48] B. Batra, S. Kumari, C.S. Pundir, Construction of glutamate biosensor based on covalent immobilization of glutmate oxidase on polypyrrole nanoparticles/polyaniline modified gold electrode, Enzyme Microb. Technol. 57 (2014) 69–77, https://doi.org/10.1016/j.enzmictec.2014.02.001.

[49] G. Hughes, R.M. Pemberton, P.R. Fielden, J.P. Hart, Development of a disposable screen-printed amperometric biosensor based on glutamate dehydrogenase, for the determination of glutamate in clinical and food applications, Anal. Bioanal. Electrochem. 6 (2014) 435–449.

[50] G. Hughes, R.M. Pemberton, P.R. Fielden, J.P. Hart, Development of a novel reagentless, screen-printed amperometric biosensor based on glutamate dehydrogenase and NAD+, integrated with multi-walled carbon nanotubes for the determination of glutamate in food and clinical applications, Sens. Actuators B Chem. 216 (2015) 614–621, https://doi.org/10.1016/j.snb.2015.04.066.